Preprints of the 8th IFAC Symposium on Advanced Control of Chemical Processes
The International Federation of Automatic Control
Furama Riverfront, Singapore, July 10-13, 2012

Model predictive control of a hybrid fuel cell & battery power system

Martin Behrendt [*] **Naim Bajcinca** [*,**] **Federico Zenith** [***] **Ulrike Krewer** [*,****]

[*] *Max Planck Institute for Dynamics of Complex Technical Systems, Sandtorstr 1, 39106 Magdeburg*
[**] *Technische Universität Berlin, Einsteinufer 17, 10587 Berlin*
[***] *Sintef Applied Cybernetics, O.S. Bragstads plass 2D, 7034 Trondheim*
[****] *Institute for Energy and Process Systems Engineering, TU Braunschweig, Franz-Liszt-Str. 35, 38106 Braunschweig*

Abstract: This paper considers optimal operation of an hybrid powered energy system. The two power sources include a direct methanol fuel cell and a lithium-ion battery. A portable system represented by characteristic dynamic load profiles is considered as the consumer. A PI and a nonlinear model predictive control algorithm have been investigated and compared in terms of efficiency and robustness of operation.

Keywords: battery, DMFC, fuel cell, nonlinear model predictive control, optimal control, portable system

1. INTRODUCTION

Providing electrical energy is one of the main problems in modern times. This task can be split into three categories: power supply for stationary, mobile and portable applications. For all three, the usage of fuel cells is a major field of research during the last years due to their advantages. Fuel cells are electrochemical energy transformers and directly provide electrical energy from chemical energy. Compared to thermal processes, fuel cells are not bound by the Carnot efficiency and therefore have the potential to use the chemical energy more efficiently.

In the field of portable applications, e.g. cell phones, notebooks and other electronic devices, the usage of lithium-ion batteries is most common. For these consumer electronics, the commercial usage of the direct methanol fuel cell (DMFC) is still a matter of research. In most of these applications the fuel cell has to operate under dynamic load demands. The main issue is that DMFCs are sensitive to dynamic operation and changes in their operation point. While short term varying behavior may have a positive effect on the performance [Park et al. (2010)], mostly attributed to cathode side oxygen starvation which leads to regeneration of the oxidised catalyst, dynamic operation may, in general, lead to increased degradation [Park et al. (2008)]. In addition, it is difficult to provide a dynamic model for the methanol concentration during a high dynamic period, as pure methanol is inserted into the stream entering the anode, leading to a delayed response time; too low concentration in the loop leads to methanol starvation on the anode and hence to catalyst oxidation and performance degradation, while methanol excess leads to increased methanol crossover, and hence to a decrease in cathode and fuel cell performance. A compromise between the dynamic operation and the lifetime duration of the fuel cell is thus necessary. Such a compromise leads to restrictions of the maximum change rate of the operation point. A second problem is that the DMFC should be as small as possible because of weight and space requirements. This is opposed by the requirement that the actual maximum load demand often is much higher then the average load, while the fuel cell should be sized on the basis of the average load. The consequence of these restrictions is, that it will not be possible to provide the energy demanded by the load at every time instant. This problem is addressed by using a battery as a buffer. If the energy output of the fuel cell is below the demand, then the battery ought to provide the additional energy, and if the fuel cell provides more energy, then the battery ought to recharge.

If the size of the fuel cell and the battery would not matter, theoretically it would be possible to operate the fuel cell at a constant level. The battery just has to be large enough. For portable applications, the size and weight however do very much matter and therefore, the components should be as small as possible. To avoid an empty or a full battery, the fuel cell has to operate dynamically. An empty battery is undesired because load demands above the operation point of the fuel cell cannot be fulfilled on time. A full state of charge is undesired because energy is wasted if the load falls below the operation point of the fuel cell. For portable devices the operational lifetime based on one fuel charge is important. Therefore, in order to assure that at every time instant every load demand is satisfied and no energy is wasted requires carfeful feedback control strategies. Additionally, an optimization of the fuel consumption could be particularly beneficial.

This paper is structured as followed. In Section 2 the hybrid power system, consisting of a DMFC and a lithium-ion battery, is presented, followed by the model and con-

troller design in Section 3. A nonlinear model predictive control (NMPC) approach is used. The performance is compared with a PI control scheme as reference. The simulation results are presented in Section 4, and a summary and outlook is given in Section 5.

2. SYSTEM MODEL

Most electronic devices operate at a constant voltage level. On the other side, the components that provide electric energy vary in the output voltage depending on the power that is provided. To be able to deliver the energy at a constant voltage DC-DC converters are used. For the presented work it is assumed that these converters are ideal and there internal dynamics can be neglected.

2.1 Fuel Cell Model

The fuel cell considered in this work is a DMFC. The DMFC is a low temperature fuel cell which is directly fed with methanol as fuel. The reactions at the anode and cathode are:

$$\text{Anode:} \quad \mathrm{CH_3OH + H_2O \rightarrow 6H^+ + 6e^- + CO_2} \quad (1a)$$

$$\text{Cathode:} \quad \frac{3}{2}\mathrm{O_2 + 6H^+ + 6e^- \rightarrow 3H_2O} \quad (1b)$$

One of the main side effects in the DMFC is the methanol crossover through the polymer electrolyte membrane. This effect is important with respect to fuel efficiency and operational lifetime because the methanol reacts with the oxygen at the cathode side resulting in a reduction of the voltage [Kamarudin et al. (2007)]. The advantages of using methanol are the easier storage compared to hydrogen and that no additional steam reforming is necessary. Another drawback of DMFCs is their sensitivity to changes in the operation point due to membrane and reaction kinetics (Gemmen and Johnson (2006); Tang et al. (2006)). Because of this sensitivity the changes in operation point of the fuel cell will be restricted such that dynamics effects can be neglected.

Figure 1 shows a general stationary voltage - current curve of a fuel cell. Working in the third region is normally avoided because the system is highly inefficient due to the load high current. Because the main operation interval is in the second quasi linear region a linear representation will be used. For more flexibility the model will represent a single cell and the cell voltage is scaled by the stack size

$$U_{\mathrm{FC}} = (U_{\mathrm{FC},0} - R_{\mathrm{FC}} \cdot I_{\mathrm{FC}}) \cdot N_{\mathrm{FC}} \quad (2)$$

with $U_{\mathrm{FC},0}$ the open cell voltage in V, R_{FC} the resistance in Ω, I_{FC} the current in A and N_{FC} the stack size.

The power of the fuel cell P_{FC} is given by:

$$P_{\mathrm{FC}} = U_{\mathrm{FC}} \cdot I_{\mathrm{FC}}. \quad (3)$$

Besides this power characteristics to represent the fuel cell also the methanol consumption is of interest. An important assumption made here is that the concentration in the fuel cell is hold constant by an internal controller. The actual fuel consumption is then resulting on the current of the fuel cell and the methanol crossover. Because we assume a constant concentration the crossover is a constant offset

$$\frac{\mathrm{d}n}{\mathrm{d}t} = c \cdot A_{\mathrm{FC}} \cdot a \cdot N_{\mathrm{FC}} + b \cdot I_{\mathrm{FC}} \cdot N_{\mathrm{FC}} \quad (4)$$

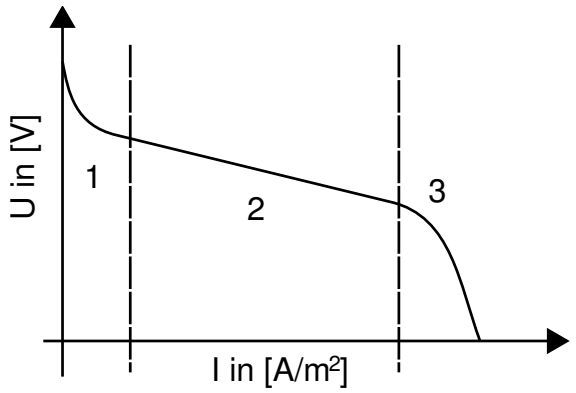

Fig. 1. General stationary voltage - current curve for a fuel cell with its three typical regions. 1: Voltage drop due activation energy required for the reaction. 2: Linear ohmic behavior. 3: Voltage drop due to transport limitations.

where n stands for the methanol consumption, c is the concentration in mol, A_{FC} is the active area and b and a are the fitting constants in $\frac{\mathrm{mol}}{\mathrm{C}}$ and $\frac{\mathrm{m}}{\mathrm{s}}$, respectively.

2.2 Battery Model

A lithium-ion battery is used as a buffer in this work. To date these type of batteries have the highest energy-mass ratio among available rechargeable batteries and represent the current standard component as energy source for portable applications. One draw back of these batteries is their sensitivity to over- and undervoltages. The cell voltage should range between 2.4 V and 4.2 V, otherwise damaging secondary reactions can occur (Pistoia (2005)).

The model presented in this work is based on Doyle et al. (1996). The configuration of the battery is, at the cathode $\mathrm{Li}_v\mathrm{Mn_2O_4}$ and at the anode $\mathrm{Li}_u\mathrm{C_6}$. u and v are stoichiometric coefficients which theoretically range between 0 and 1. Because of different effects like an initial concentration in the manganese dioxide electrode the real values vary. Detailed information are given in Doyle et al. (1996). The values chosen for this work and the corresponding state of charge are given in Table 1.

Table 1. Minimum and maximum lithium stoichiometric coefficients representing the *SoC*

SoC	0	1
u	0.0045	0.57
v	0.80	0.17

The empiric equations for the open cell potentials (E_0) are given as:

$$\begin{aligned} E_0^+ = {} & 4.19829 + 0.0565661 \cdot \tanh\left(-14.5546 \cdot v + 8.60942\right) \\ & - 0.0275479 \cdot \left(\frac{1}{(0.998432 - v)^{0.492465}} - 1.90111\right) \\ & - 0.157123 \cdot \exp\left(-0.04738 \cdot v^8\right) \\ & + 0.810239 \cdot \exp\left(-40 \cdot (v - 0.133875)\right) \end{aligned} \quad (5a)$$

$$\begin{aligned} E_0^- = {} & -0.16 + 1.32 \cdot \exp\left(-3.0 \cdot u\right) \\ & + 10 \cdot \exp\left(-2000.0 \cdot u\right). \end{aligned} \quad (5b)$$

The open cell voltage is:

$$U_{\mathrm{Bt},0} = E_0^+ - E_0^-. \tag{6}$$

Charging or discharging the battery results in overpotentials at the anode and cathode. These are described by the Butler Volmer kinetics [Newman and Thomas-Alyea (2004)]

$$\begin{aligned} I_{\mathrm{Bt}} = I_0^{\pm} \cdot \Bigg[& \exp\left(\frac{\alpha_{\pm} \cdot F}{R \cdot T} \cdot \eta^{\pm}\right) \\ & - \exp\left(-\frac{(1-\alpha_{\pm}) \cdot F}{R \cdot T} \cdot \eta^{\pm}\right)\Bigg] \end{aligned} \tag{7}$$

where I_{Bt} is the battery current in A, $I_0^{\pm}$ the exchange current in A, η the overpotential in V, T the Temperature in K (which will be assumed constant) and F, R the Faraday and universal gas constant in $\frac{\mathrm{As}}{\mathrm{mol}}$ and $\frac{\mathrm{J}}{\mathrm{mol \cdot K}}$, respectively. α is a symmetry factor and the most common choice is $\alpha = 0.5$. By summarizing the constants in the exponent

$$k = \frac{0.5 \cdot F}{R \cdot T} \tag{8}$$

and

$$\sinh(x) = \frac{\mathrm{e}^{x} - \mathrm{e}^{-x}}{2} \tag{9}$$

(7) can be solved for the overvoltage explicitly

$$\eta = \frac{1}{k} \cdot \operatorname{arsinh}\left(\frac{I}{2 \cdot I_0}\right). \tag{10}$$

With

$$P_{\mathrm{Bt}} = U_{\mathrm{Bt}} \cdot I_{\mathrm{Bt}} \cdot N_{\mathrm{Bt}} \tag{11}$$

we obtain an implicit equation to calculate the battery current

$$\begin{aligned} 0 = I_{\mathrm{Bt}} \Bigg(& U_{\mathrm{Bt},0} + \frac{1}{k^+} \cdot \operatorname{arsinh}\left(\frac{I_{\mathrm{Bt}}}{2 \cdot I_0^+}\right) \\ & - \frac{1}{k^-} \cdot \operatorname{arsinh}\left(\frac{I_{\mathrm{Bt}}}{2 \cdot I_0^-}\right)\Bigg) - \frac{P_{\mathrm{Bt}}}{N_{\mathrm{Bt}}}. \end{aligned} \tag{12}$$

The battery power for one cell can be written in terms of the fuel cell power output and the load

$$P_{\mathrm{Bt}} = \frac{P_{\mathrm{L}} - (U_{\mathrm{FC},0} - R_{\mathrm{FC}} \cdot I_{\mathrm{FC}}) \cdot I_{\mathrm{FC}} \cdot N_{\mathrm{FC}}}{N_{\mathrm{Bt}}}. \tag{13}$$

From the battery current, the change in the state of charge can be obtained with a simple ordinary differential equation

$$\frac{\mathrm{d}SoC}{\mathrm{d}t} = -\frac{1}{C_{\mathrm{Bt}}} \cdot I_{\mathrm{Bt}} \tag{14}$$

where C_{Bt} represents the maximum battery capacity in As.

The simulation model is:

$$\frac{\mathrm{d}n}{\mathrm{d}t} = c \cdot A_{\mathrm{FC}} \cdot a \cdot N_{\mathrm{FC}} + b \cdot I_{\mathrm{FC}} \cdot N_{\mathrm{FC}} \tag{15a}$$

$$\frac{\mathrm{d}SoC}{\mathrm{d}t} = -\frac{1}{C_{\mathrm{Bt}}} \cdot I_{\mathrm{Bt}} \tag{15b}$$

$$\begin{aligned} 0 = I_{\mathrm{Bt}} \Bigg(& U_{\mathrm{Bt},0} - \frac{1}{k^+} \cdot \operatorname{arsinh}\left(\frac{I_{\mathrm{Bt}}}{2 \cdot I_0^+}\right) \\ & - \frac{1}{k^-} \cdot \operatorname{arsinh}\left(\frac{I_{\mathrm{Bt}}}{2 \cdot I_0^-}\right)\Bigg) \\ & - \frac{P_{\mathrm{L}} - (U_{\mathrm{FC},0} - R_{\mathrm{FC}} \cdot I_{\mathrm{FC}}) \cdot I_{\mathrm{FC}} \cdot N_{\mathrm{FC}}}{N_{\mathrm{Bt}}}. \end{aligned} \tag{15c}$$

2.3 Discretized Model

For the NMPC, a discrete version of the model is required. For the state of charge, a simple Newton approximation is used

$$SoC(\mathrm{k}+1) = SoC(\mathrm{k}) + \frac{1}{C_{\mathrm{Bt}}} \cdot I_{\mathrm{Bt}} \cdot \Delta t. \tag{16}$$

The methanol consumption will not be predicted and in (15c) the open cell voltage $U_{\mathrm{Bt},0}$ will be linearized

$$U_{\mathrm{Bt},0} = 1.5666 \cdot SoC + 2.8798. \tag{17}$$

3. CONTROLLER DESIGN

Figure 2 shows the principal feedback control scheme. The Controller C (e.g. a PI one) sees only the difference of the state of charge SoC to the set-point. As output is the operation point for the fuel cell which can be seen as an actuator. The load represents effectively a disturbance and the difference between load and fuel cell power output is the input for the battery, affecting the state of charge SoC.

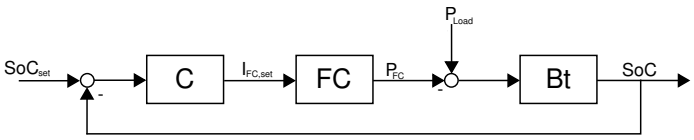

Fig. 2. Feedback control scheme.

The NMPC algorithm respects a slightly different control scheme, as it does not have a specified level SoC_{set}. In this article we adopt the algorithm from Sutton and Bitmead (2000). We will avoid a detailed derivation of the equations from the given sources and restrict us to the important modifications.

Consider a discrete model given by

$$\mathbf{x}_{\mathrm{k}+1} = \mathbf{f}_{\mathrm{d}}(\mathbf{x}_{\mathrm{k}}, \mathbf{u}_{\mathrm{k}}) \tag{18a}$$

$$\mathbf{y}_{\mathrm{k}} = \mathbf{h}_{\mathrm{d}}(\mathbf{x}_{\mathrm{k}}). \tag{18b}$$

The original cost function J for the optimization is extended by a vector of Lagrange multipliers $\boldsymbol{\lambda}$,

$$\begin{aligned} J = \phi(\mathbf{x}_{\mathrm{N}}) + \sum_{\mathrm{k}=0}^{\mathrm{N}-1} \Big[& L(\mathbf{e}_{\mathrm{k}}, \mathbf{u}_{\mathrm{k}}, \Delta\mathbf{u}_{\mathrm{k}}) \\ & + \boldsymbol{\lambda}_{\mathrm{k}+1}^{\mathrm{T}} \cdot (\underbrace{\mathbf{f}_{\mathrm{d}}(\mathbf{x}_{\mathrm{k}}, \mathbf{u}_{\mathrm{k}}) - \mathbf{x}_{\mathrm{k}+1}}_{=0 \ (18a)}) \Big] \end{aligned} \tag{19}$$

with

$$\mathbf{e} := \mathbf{y}_{\mathrm{set}} - \mathbf{y} = \mathbf{y}_{\mathrm{set}} - \mathbf{h}_{\mathrm{d}}(\mathbf{x}) \tag{20a}$$

$$\phi(\mathbf{x}_{\mathrm{N}}) := \frac{1}{2} \mathbf{e}_{\mathrm{N}}^{\mathrm{T}} \mathbf{P} \mathbf{e}_{\mathrm{N}} \tag{20b}$$

$$\begin{aligned} L(\mathbf{e}_{\mathrm{k}}, \mathbf{u}_{\mathrm{k}}, \Delta\mathbf{u}_{\mathrm{k}}) := \frac{1}{2} \Big[& \mathbf{e}_{\mathrm{k}}^{\mathrm{T}} \mathbf{Q} \mathbf{e}_{\mathrm{k}} \\ & + \mathbf{u}_{\mathrm{k}}^{\mathrm{T}} \mathbf{R} + \Delta\mathbf{u}_{\mathrm{k}}^{\mathrm{T}} \mathbf{T} \Delta\mathbf{u}_{\mathrm{k}} \Big] \end{aligned} \tag{20c}$$

$$\Delta\mathbf{u}_{\mathrm{k}} := \mathbf{u}_{\mathrm{k}-1} - \mathbf{u}_{\mathrm{k}}, \tag{20d}$$

where $\{\mathbf{P}, \mathbf{Q}, \mathbf{R}, \mathbf{T}\} \geq 0$ are weight matrices. The Hamiltonian is defined as

$$H_{\mathrm{k}} := L(\mathbf{e}_{\mathrm{k}}, \mathbf{u}_{\mathrm{k}}, \Delta\mathbf{u}_{\mathrm{k}}) + \boldsymbol{\lambda}_{\mathrm{k}+1}^{\mathrm{T}} \cdot \mathbf{f}_{\mathrm{d}}(\mathbf{x}_{\mathrm{k}}, \mathbf{u}_{\mathrm{k}}). \tag{21}$$

Equation (21) is solved for $L(\mathbf{e}_{\mathrm{k}}, \mathbf{u}_{\mathrm{k}}, \Delta\mathbf{u}_{\mathrm{k}})$ and substituted in (19). The total derivative of the resulting equation is

computed to obtain the optimum. It turns out that the following choices for the costates $\boldsymbol{\lambda}_\mathrm{k}$

$$\boldsymbol{\lambda}_\mathrm{N}^\mathrm{T} := \frac{\partial \phi}{\partial \mathbf{x}_\mathrm{N}} = -\mathbf{e}_\mathrm{N}^\mathrm{T}\mathbf{P} \cdot \frac{\mathrm{d}\mathbf{h}_\mathrm{d}(\mathbf{x}_\mathrm{N})}{\mathrm{d}\mathbf{x}_\mathrm{N}} \tag{22a}$$

$$\begin{aligned}\boldsymbol{\lambda}_\mathrm{k}^\mathrm{T} &:= \frac{\partial H_\mathrm{k}}{\partial \mathbf{x}_\mathrm{k}} + \frac{\partial H_\mathrm{k}}{\partial \mathbf{e}_\mathrm{k}}\frac{\partial \mathbf{e}_\mathrm{k}}{\partial \mathbf{x}_\mathrm{k}} \\ &= \boldsymbol{\lambda}_{\mathrm{k}+1}^\mathrm{T}\frac{\partial \mathbf{f}_\mathrm{d}(\mathbf{x}_\mathrm{x}, \mathbf{u}_\mathrm{k})}{\partial \mathbf{x}_\mathrm{k}} - \mathbf{e}_\mathrm{k}^\mathrm{T}\mathbf{Q} \cdot \frac{\mathrm{d}\mathbf{h}_\mathrm{d}(\mathbf{x}_\mathrm{k})}{\mathrm{d}\mathbf{x}_\mathrm{k}}\end{aligned} \tag{22b}$$

simplify the total derivative to

$$\mathrm{d}J = \sum_{\mathrm{k}=0}^{\mathrm{N}-1}\frac{\partial H_\mathrm{k}}{\partial \mathbf{u}_\mathrm{k}}\mathrm{d}\mathbf{u}_\mathrm{k} + \boldsymbol{\lambda}_0^\mathrm{T}\mathrm{d}\mathbf{x}_0. \tag{23}$$

$\frac{\partial H_\mathrm{k}}{\partial \mathbf{u}_\mathrm{k}}$ is the gradient of J with respect to $\mathbf{u}_\mathrm{k}$ with $\mathbf{u}_{\mathrm{j},\mathrm{j}\neq\mathrm{i}}$ and $\mathbf{x}_0$ kept constant. If a (local) minimum for J is reached, then $\frac{\partial H_\mathrm{k}}{\partial \mathbf{u}_\mathrm{k}} = 0$ holds. This means that a further change in the input $\mathbf{u}$ does not effect the Hamiltonian anymore.

To solve the optimization problem the gradient $\frac{\partial H_\mathrm{k}}{\partial \mathbf{u}_\mathrm{k}}$ is computed by

$$\frac{\partial H_\mathrm{k}}{\partial \mathbf{u}_\mathrm{k}} = \mathbf{R} - \Delta\mathbf{u}_\mathrm{k}^\mathrm{T}\mathbf{T} + \boldsymbol{\lambda}_{\mathrm{k}+1}^\mathrm{T}\frac{\partial \mathbf{f}(\mathbf{x}_\mathrm{k}, \mathbf{u}_\mathrm{k})}{\partial \mathbf{u}_\mathrm{k}} \tag{24}$$

while $\mathbf{u}_\mathrm{k}$ are updated by moving along this gradient. Kim et al. (2002) proposed an iterative scheme for the solution of the optimization problem:

while $\Delta J \geq \epsilon$
  for $k = 1, ..., \mathrm{N}$
    compute $\mathbf{x}_\mathrm{k}$ using (18a)
  end
  for $k = \mathrm{N}, ..., 1$
    compute $\boldsymbol{\lambda}_\mathrm{k}$ using (22a) and (22b)
  end
  for $k = 0, ..., \mathrm{N}-1$
    compute $\frac{\partial H_\mathrm{k}}{\partial \mathbf{u}_\mathrm{k}}$ using (24)
  end
  if $\Delta J \leq 0$
    $\mathbf{u}_{\mathrm{k,new}} := \mathbf{u}_{\mathrm{k,old}} - \Delta_\mathrm{k}\frac{\partial H_\mathrm{k}}{\partial \mathbf{u}_\mathrm{k}}$ for $k = 0, .., \mathrm{N}-1$
  else reduce Δ_k
end while.

Here ϵ is a breaking criteria and Δ_k a scaling factor for the update.

For the underlying problem presented in Section 2 the following substitutions hold:

- $x = SoC$
- $u = I_\mathrm{FC}$
- $e = \begin{cases} SoC_\mathrm{max} - x & \text{for } SoC \geq SoC_\mathrm{max} \\ SoC_\mathrm{min} - x & \text{for } SoC \leq SoC_\mathrm{min} \\ 0 & \text{otherwise} \end{cases}$
  with the assumption that the state of charge can be measured directly ($\mathbf{y} = \mathbf{x}$).

The error e defines a band where the system can move freely. Only too high or too low states of charge shall be avoided and therefore are penalized in the cost function

$$\begin{aligned}J = &\frac{1}{2}\mathbf{e}_\mathrm{N}^\mathrm{T}\mathbf{P}\mathbf{e}_\mathrm{N} \\ &+ \sum_{\mathrm{k}=1}^{\mathrm{N}-1}\left[\frac{1}{2}\left[\mathbf{e}_\mathrm{k}^\mathrm{T}\mathbf{Q}\mathbf{e}_\mathrm{k} + 2\mathbf{u}_\mathrm{k}^\mathrm{T}\mathbf{R} + \Delta\mathbf{u}_\mathrm{k}^\mathrm{T}\mathbf{T}\Delta\mathbf{u}_\mathrm{k}\right]\right].\end{aligned} \tag{25}$$

A second cost function will be of interest. The cost function is extended by a second error term. This error is calculated by

$$s = u_\mathrm{set} - u. \tag{26}$$

The set-point is the average load

$$u_\mathrm{set} = \frac{1}{t}\cdot\int_0^t w(\tau)\mathrm{d}t. \tag{27}$$

The changes in the algorithm are

$$\begin{aligned}J = \frac{1}{2}\mathbf{e}_\mathrm{N}^\mathrm{T}\mathbf{P}\mathbf{e}_\mathrm{N} + \sum_{\mathrm{k}=1}^{\mathrm{N}-1}\Bigg[\frac{1}{2}\big[&\mathbf{e}_\mathrm{k}^\mathrm{T}\mathbf{Q}\mathbf{e}_\mathrm{k} + 2\mathbf{u}_\mathrm{k}^\mathrm{T}\mathbf{R} \\ &+ \Delta\mathbf{u}_\mathrm{k}^\mathrm{T}\mathbf{T}\Delta\mathbf{u}_\mathrm{k} + \mathbf{s}_\mathrm{k}^\mathrm{T}\mathbf{S}\mathbf{s}_\mathrm{k}\big]\Bigg]\end{aligned} \tag{28}$$

and

$$\frac{\partial H_\mathrm{k}}{\partial \mathbf{u}_\mathrm{k}} = -\mathbf{R} - \Delta\mathbf{u}_\mathrm{k}^\mathrm{T}\mathbf{T} - \mathbf{s}_\mathrm{k}\mathbf{S} + \boldsymbol{\lambda}_{\mathrm{k}+1}^\mathrm{T}\frac{\partial \mathbf{f}(\mathbf{x}_\mathrm{k}, \mathbf{u}_\mathrm{k})}{\partial \mathbf{u}_\mathrm{k}}. \tag{29}$$

4. SIMULATION RESULTS

4.1 Simulation parameters

Problem data are given in the following table:

Variable	Value	Unit	Variable	Value	Unit
A_Bt	28e-4	m^2	N_Bt	3	-
A_FC	26e-4	m^2	N_FC	20	-
$\alpha_\pm$	0.5	-	R	0.95	$\frac{\mathrm{J}}{\mathrm{kg}\cdot\mathrm{K}}$
C_Bt	0.95	Ah	R_FC	0.0533	Ω
F	96487	$\frac{\mathrm{C}}{\mathrm{mol}}$	SoC_init	0.4	-
I_0^+	0.11	$\frac{\mathrm{mA}}{\mathrm{cm}^2}$	SoC_max	0.45	-
I_0^-	0.08	$\frac{\mathrm{mA}}{\mathrm{cm}^2}$	SoC_min	0.35	-
$I_\mathrm{Fc,max}$	4.5	A	SoC_set	0.4	-
$I_\mathrm{Fc,min}$	0	A	T	297.15	K
$\Delta I_\mathrm{Fc,max}$	0.005	$\frac{\mathrm{A}}{\mathrm{s}}$	$U_\mathrm{FC,0}$	0.6	V

while the following controller settings have been used for the simulations:

Variable	Value	Unit	Variable	Value	Unit
K_P	7	A	$\mathbf{R}$	0.5	-
T_N	1400	s	$\mathbf{S}$	100	-
$\mathbf{P}$	300	-	$\mathbf{T}$	150	-
$\mathbf{Q}$	200	-			

K_P is the gain and T_N the integrator time constant of the PI controller.

4.2 Load profiles

For the simulations different load scenarios were used for the evaluation. For boot-up scenarios constant loads were assumed to inspect the stationary behavior. Figure 3 shows three different profiles used for the simulations. The main difference in the scenarios is the frequency of the changes in the load. Scenario 1 is the most calm one, Scenario 3 has the fastest changes.

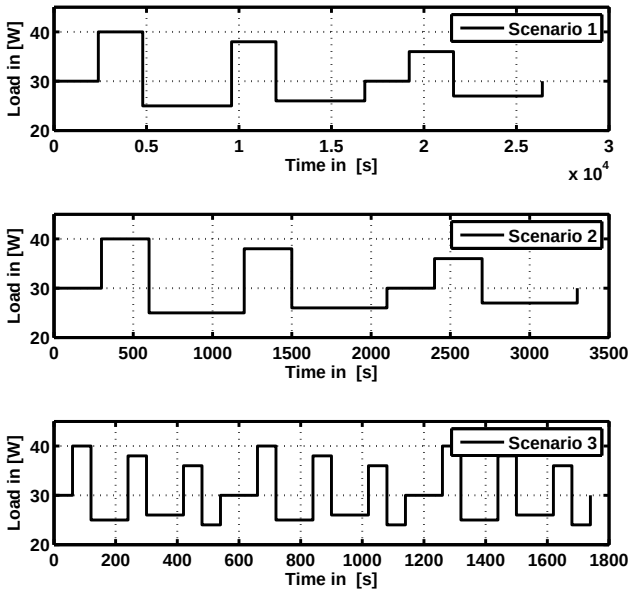

Fig. 3. Different basic load profiles used for the simulations.

4.3 Results

In general it can be noted that both controllers have a similar performance. For Scenario 1 the results are shown in Figure 4 - 6. The main difference is that the NMPC reacts faster and changes the set point of the fuel cell more frequently. As a result of that the SoC stays in a smaller band. Because the PI controller reacts slow the constraints for the battery cell voltage are violated. Besides this both controllers show a similar performance and the fuel consumption is in the same range.

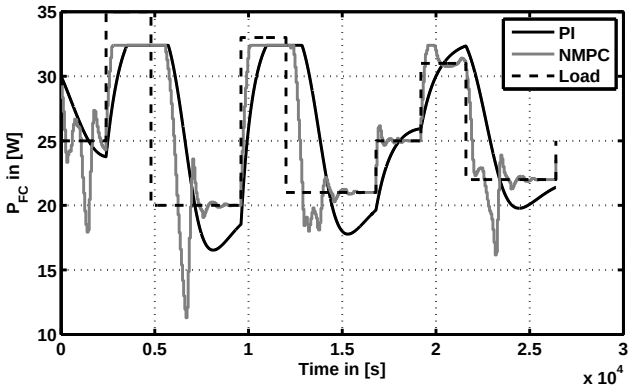

Fig. 4. Fuel cell power output for Scenario 1 of the PI controller and the NMPC with the cost function (25).

Table 2 shows the consumed methanol for the three scenarios and the state of charge at the end of the simulation. Scenario 1 and 3 have a lower amount of consumed methanol for the NMPC. But also the SoC at the end of the simulation is lower. For Scenario 2 the SoC is similar and the simulation with the PI controller has a lower methanol consumption. It can be noted that in terms of methanol efficiency both controllers show a similar performance but the PI controller violates constraints for one of the three considered scenarios. If the PI controller

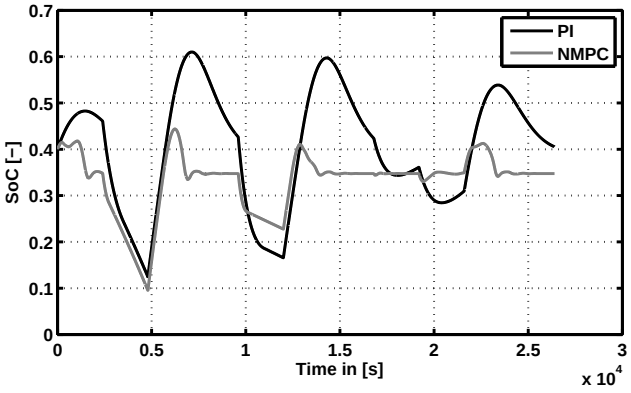

Fig. 5. State of charge for Scenario 1.

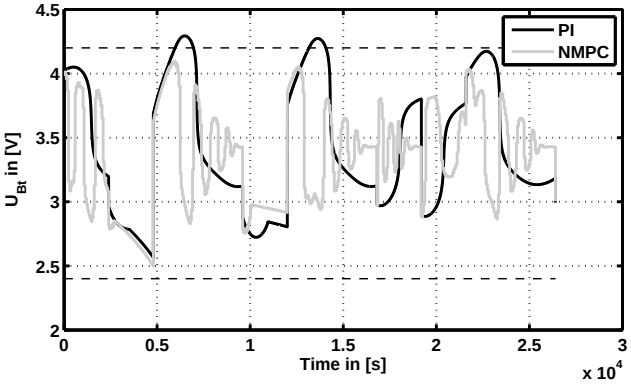

Fig. 6. Battery cell voltages for Scenario 1.

is used, the fuel cell experiences slower changes of the operation point. An advantage of the NMPC can be observed in Fig. 5. The PI controller has a SoC varying between 0.6 and 0.1, the NMPC between 0.45 and 0.1, implying that batteries for NMPC can be designed at a smaller size, since they need to accomodate a smaller oscillation, and can thereby be up to 30% lighter.

Table 2. Comparison of the methanol consumption and SoC at the end of a simulation. The state of charge is given in % and the consumed methanol in mol.

		Scenario 1	Scenario 2	Scenario 3
SoC_{end}	NMPC	34.76	42.64	35.72
	PI	40.53	42.24	40.47
n	NMPC	17.941	5.824	5.598
	PI	18.242	5.627	5.614

To improve the NMPC the second cost function (28) is introduced. The average load changes not as fast and therefore the fuel cell should be operated more smooth. Figure 7 - 9 show the power output of the fuel cell for the 3 scenarios. The introduced set point for the input u shows the desired effect. The corresponding methanol consumption is given in Table 3. For all scenarios the change in the cost function results in a better methanol consumption. The NMPC is still operating the fuel cell more dynamically than the PI controller but compared to the first NMPC approach improvements have been made.

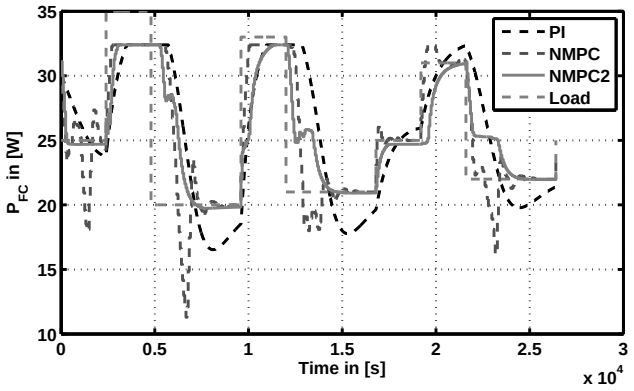

Fig. 7. Comparison of the fuel cell power output for Scenario 1.

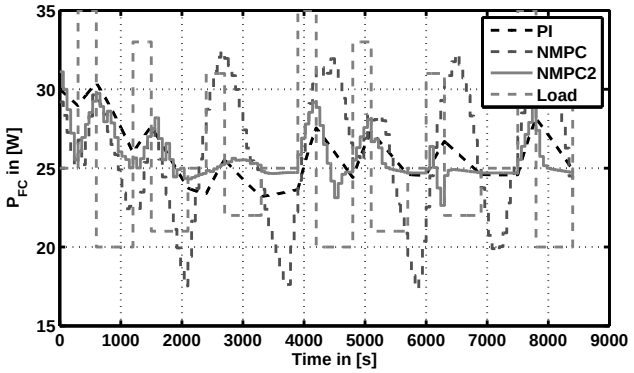

Fig. 8. Comparison of the fuel cell power output for Scenario 2.

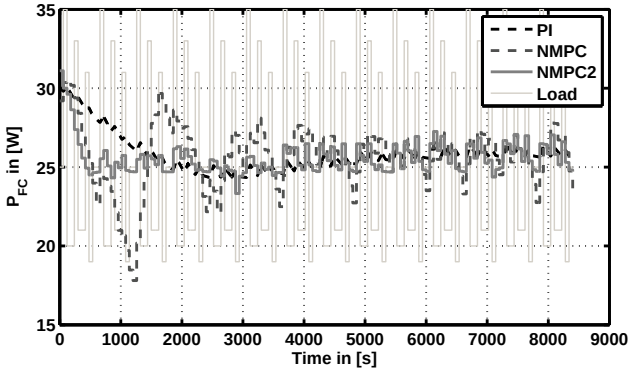

Fig. 9. Comparison of the fuel cell power output for Scenario 3.

Table 3. Comparison of the consumed methanol for the three scenarios and the considered control algorithms.

	PI	NMPC	NMPC2
Scenario 1	18.242	17.941	17.854
Scenario 2	5.627	5.824	5.590
Scenario 3	5.614	5.598	5.545

5. CONCLUSION

A hybrid power system including a direct methanol fuel cell (DMFC) and a lithium-ion battery is presented in conjunnction with two different control schemes. A PI control and a model predictive control (NMPC) scheme are compared with respect to the fuel consumption efficiency. While PI control provides already a good efficiency, it may violate the operation constraints. It is shown that the battery voltage exceeds the maximum allowed cell voltage in some cases. Unless the energy is properly dissipated, the battery may undergo damage. Two cost functions settings have been considered for the model predictive control scheme. In both cases the problem of the overvoltage is avoided. While in the first setting a comparable fuel efficiency to the PI control scheme is achieved, in the second setting a change of the cost function leads to a better efficiency and to a smoother operation of the fuel cell. While other problem data may provide different quantitative observations, the main purpose of this work has been to demonstrate the advantages resulting from "intelligent" principle feedback control schemes as opposed to heuristic non-programmatic approaches often encountered in practice.

REFERENCES

Allgower, F. and Zheng, A. (eds.) (2000). *Nonlinear Model Predictive Control (Progress in Systems & Control Theory Vol.26)*. Birkhauser Verlag.

Doyle, M., Newman, J., Gozdz, A., Schmutz, C., and Tarascon, J. (1996). Comparison of modeling predictions with experimental data from plastic lithium ion cells. *Journal of the Electrochemical Society*, 143(6), 1890–1903.

Gemmen, R.S. and Johnson, C.D. (2006). Evaluation of fuel cell system efficiency and degradation at development and during commercialization. *Journal of Power Sources*, 159(1), 646–655.

Kamarudin, S.K., Daud, W.R.W., Ho, S.L., and Hasran, U.A. (2007). Overview on the challenges and developments of micro-direct methanol fuel cells (dmfc). *Journal of Power Sources*, 163(2), 743–754.

Kim, H., Shim, D., and Sastry, S. (2002). Nonlinear model predictive tracking control for rotorcraft-based unmanned aerial vehicles. In *Proceedings of the 2002 American Control Conference*, volume 1-6, 3576–3581. IEEE.

Newman, J. and Thomas-Alyea, K. (2004). *Electrochemical systems*. Wiley-Interscience.

Park, J.Y., Lee, J.H., and Son, I.h. (2008). The operating mode dependence on electrochemical performance degradation of direct methanol fuel cells. *Int. Journal of Hydrogen Energy*, 195, 4833–4843.

Park, Y.C., Peck, D.H., Kim, S.K., Lim, S., Jung, D.H., Jang, J.H., and Lee, D.Y. (2010). Dynamic response and long-term stability of a small direct methanol fuel cell stack. *Journal of Power Sources*, 195, 4080–4089.

Pistoia, G. (2005). *Batteries for portable devices*. Elsevier Science.

Sutton, G. and Bitmead, R. (2000). Performance and computational implementation of nonlinear model predictive control on a submarine. volume 26, 461–472. In Allgower and Zheng (2000).

Tang, Y., Santare, M., Karlsson, A., Cleghorn, S., and Johnson, W. (2006). Stresses in proton exchange membranes due to hygro-thermal loading. *Journal of Fuel Cell Science and Technology*, 3(2), 119–124.